Microscopic dynamics of liquid gallium

F. J. Bermejo,[1] M. García-Hernández,[1] J. L. Martinez,[2] and B. Hennion[3]
[1]*Instituto de Estructura de la Materia, Consejo Superior de Investigaciones Científicas, Serrano 123, E-28006 Madrid, Spain*
[2]*Instituto de Ciencia de Materiales, Consejo Superior de Investigaciones Científicas, Facultad de Ciencias, C-IV, Universidad Autónoma de Madrid, E-28049 Madrid, Spain*
[3]*Laboratoire Leon Brillouin, Centre de Etudes de Saclay, 91191 Gif-sur-Yvette Cedex, France*
(Received 19 November 1993)

The microscopic dynamics of liquid Ga is investigated by means of inelastic neutron scattering. The analysis of the experimental intensities is carried out with the help of available effective potentials derived from direct inversion of the static structure factors, and the absence of well defined collective excitations explained in terms of the relatively high values of the longitudinal viscosity. The relevance of the present findings regarding some electronic transport processes is finally discussed.

PACS number(s): 62.10.+s, 72.15.Cz

I. INTRODUCTION

Although a consistent picture concerning the microscopic collective dynamics of simple liquid metals such as the molten alkali metals [1] and group IV elements such as liquid lead [2] has emerged in the last couple of decades, both the microscopic structure and dynamics of semimetals such as Ga, In, or Ge are still somewhat controversial. As a matter of fact, two explanations of the strongly asymmetric first liquid diffraction peak have emerged, portraying such a feature as arising from an interplay of two different length scales associated with the diameter of the repulsive core and the Friedel wavelength ($\lambda_F = 2\pi/k_F$), respectively [3], or from the partial-covalency effects [4], which, in the case of liquid and amorphous [5] Ga, could become specially important.

The case of liquid Ga deviates somewhat from the simple-liquid character, since a behavior resembling that observed for the heavy alkali-metal elements Rb [6] and Cs [7] could be expected from its "harmonic liquid" macroscopic constants [8]. Even more, a direct calculation of the first even-frequency moments of the $S(Q,\omega)$ dynamic structure factors using as input data the experimental $S(Q)$ structure factors and effective potentials, as reported in the Appendix, reveals that well defined excitations at finite frequencies could be expected to occur below wave vectors of $Q \approx 1.7$ Å^{-1}, where $Q = (4\pi/\lambda)\sin(\theta/2)$. The present paper aims to contribute toward the clarification of such facts by means of the analysis of the inelastic-scattering intensity of liquid Ga carried out at a thermodynamic state equivalent to one of the two cases analyzed by Bellisent-Funel *et al.* [9], where an effective two-particle potential was derived from inversion of the measured $S(Q)$ static structure factor. The availability of such a potential thus enables the prediction of several quantities which characterize the thermal motion of the liquid, assuming that this conforms to a simple-liquid behavior, an assumption which can be tested by comparison with the corresponding quantities as derived from experiment.

Understanding the dynamic structure factor also helps to define some of the most relevant electronic transport properties, such as the electrical resistivity. Our interest in this particular topic is focused on the analysis of the relative importance of the quasielastic and inelastic contributions to $S(Q,\omega)$, a point seldom addressed in the literature regarding electronic conduction in liquids.

Although some previous neutron measurements on the same material have been previously reported in the literature, the focus of such studies was centered on either the inelastic structure factors at constant energy transfers [10], or in the low-energy (quasielastic) scattering in the supercooled region [11], precluding comparison of the experimental dynamic structure factors with the calculated ones for the kinematic range of interest.

II. EXPERIMENTAL DETAILS

The neutron measurements were carried out using the 1T thermal triple-axis spectrometer of the Orpheé reactor at the Laboratoire Leon Brillouin, Saclay (France). All the measurements were carried out in the constant k_f mode using incident wave vectors of 2.66 Å^{-1} and 4.03 Å^{-1}. Although a somewhat larger incident wave vector would be more adequate to cover a broader kinematic range, the two values quoted above represent a compromise between an acceptable resolution in energy transfers (i.e., to separate the quasielastic component) and a moderate coverage of the energy transfers of interest. The beam collimation employed was of 60′ (in pile) 40′ (monochromator) 50′ monochromator to sample and 60′ (sample to analyzer), providing resolutions in energy transfers of 0.2 THz and 0.74 THz full width at half maximum (FWHM) as measured with a vanadium standard. Several different runs were carried out on the constant-Q mode using the two referenced wave vectors, as well as on the constant energy-transfer mode. Also, the elastic intensity $I(Q,\omega=0)$ was measured several times between runs in order to ascertain the stability of the sample. The sample (electronics grade Ga, provided by Professor F. Briones) was placed inside a niobium cylinder of 1 cm diam with 0.5 mm thick walls and a height of 47 mm.

The temperature during the measurements was kept approximately constant at 330 K. The data were converted into dynamic structure factors and the measured $S(Q)$ [9] were used for normalization. Sample absorption was corrected using our own code, and special care was put into the correction for multiple scattering. Because of the widespread values found in the literature for the incoherent cross section (for a tabulation see Ref. [9]) it was difficult to model from scratch a scattering kernel to be used in the Monte Carlo calculations carried out using the DISCUS code [12]. The total (integrated in energy) percentage of multiply scattered neutrons was first estimated from a run of the code and comparing the results for $S(Q)$ after applying a correction following the factor method, with the tabulated one measuring T=326 K [9]. After some iterations the estimated percentage of multiply scattered neutrons was of 12% and 17% for the two referenced incident wave vectors. Once the total percentage of multiply scattered neutrons was set, several different scattering kernels were modeled using a scattering law for the input $S(Q,\omega)$ based upon the three-pole approximation (see Appendix) and the Kerr formula to relate the self-scattering to the total [13] (see below). The values of the total (integrated in energy and momentum) cross section were then varied until the percentage of multiple scattering (integrated in energy) matched the values given above. The spectra were subsequently corrected with the distributions estimated in such a way. In order to obtain the values of the $S(Q,0)$ elastic intensities, the measured quantities were corrected from the resolution effects in a straightforward manner. No accurate estimate of the generalized frequency distribution can be derived from an experiment of the kind reported here (for a basically total coherent scattering sample), and, moreover, the absence of suitable isotopes preempts any possibility of measuring the incoherent scattering spectra. In order to derive quantities which could be qualitatively compared with the calculated result, the following functions (i.e., related to the longitudinal current-current correlation function)

$$P(Q,\omega) = \frac{2m_i\omega}{\hbar^2 Q^2}[n(\omega)+1]^{-1}S(Q,\omega), \tag{1}$$

where $n(\omega)$ represents a Bose factor and m_i the atomic mass, were calculated from the experimental results. For relatively large momentum transfers (i.e., well beyond the first diffraction peak), the resolution effects are minimized, since the quasielastic widths far exceed the achieved resolution and, moreover, they can be compared with the calculated $Z(\omega)$ on qualitative grounds (i.e., assuming that the incoherent approximation holds, and ignoring the details of the low-frequency dynamics related to mass diffusion). Spectra measured at constant momentum transfers for $Q = 5$ Å^{-1} are then used for such a purpose.

III. RESULTS AND DISCUSSION

A. Elastic scattering

The aim of this section is to compare estimates of the $\eta(Q,0)$ longitudinal viscosity derived from experimental quantities according to well established formulas [14, 15] with that calculated from the structure factor and effective potential, assuming a simple-liquid behavior. The definition of longitudinal viscosity follows Ref. [14], where the mass density term [16] has been incorporated to convert from kinematic viscosity, and is written in terms of elastic and static quantities as

$$\eta(Q,0) = \pi\rho_i m_i v_{\rm th}^2 \frac{S(Q,\omega=0)}{S(Q)^2}, \tag{2}$$

$$\eta(0,0) = \frac{4}{3}\eta_s + \eta_B, \tag{3}$$

where ρ_i is the ionic number density, m_i the particle mass, $v_{\rm th}$ is the thermal velocity, $S(Q,\omega=0)$ represents strictly elastic scattering, and the hydrodynamic limit reproduces the total viscosity given in terms of its shear and bulk components. Alternatively, an estimate of the longitudinal viscosity can be derived from the calculated second $\omega_0^2(Q)$ and fourth $\omega_l^2(Q)$ reduced frequency moments and the associated Maxwellian relaxation time $\tau(Q)$ (see Appendix) as

$$\eta_{\rm calc}(Q,0) = \frac{\rho_i m_i}{Q^2}[\omega_0^2(Q) - \omega_l^2(Q)]\tau(Q). \tag{4}$$

The functions derived from the present measurement are shown in Fig. 1, for the two sets of experiments using different resolutions in energy transfers, and are compared with the calculated quantity. As can be seen, both functions can nearly be superimposed within the range of explored wave vectors. The statistical quality of the data deteriorates substantially below 1 Å^{-1} due to the low counting intensities in such a range (i.e., the value of $S(Q)$ is of the order of ≈ 0.008 for the two data points shown in that region). The hydrodynamic limit is obviously difficult to guess from such steep curves, but seems to lie certainly higher than $(4/3)\eta_s = 2.5$ cP as calculated

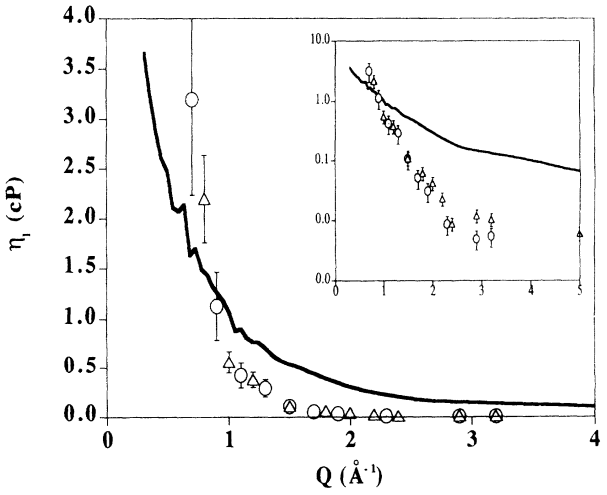

FIG. 1. Experimental and calculated $\eta(Q,0)$ longitudinal viscosities. Circles represent the data measured using a final $k_f = 4.03$ Å^{-1} and triangles refer to data measured with $k_f = 2.66$ Å^{-1}. The solid line represents the calculated result (see text). The inset shows the same quantities extending up to $Q = 5$ Å^{-1} plotted on a logarithmic scale.

from the experimental value [17]. The fact that such a behavior is followed by both the experimental and calculated quantities gives support to the idea that a substantial contribution from the η_B bulk coefficient should be operative within this range of wave vectors. Such a finding is in agreement with data reported for other liquid metals such as lead and bismuth [18], where hydrodynamic values of about 4.5 cP and 10 cP were found to be consistent with those derived from neutron scattering and computer simulation data, which extrapolates to the correct hydrodynamic limit [19]. On the other hand, the comparison of experimental and calculated quantities evidence a clearly different trend, since the curvature of the latter curve is substantially less pronounced than those derived from experiment. In particular, visual extrapolation of the calculated curve leads to a value of about 5.2 cP, not too different from that of lead, where collective excitations have been evidenced [2], whereas values one order of magnitude larger are estimated from the experimental curves. The present finding is thus reminiscent of that regarding the well documented case of liquid bismuth [18, 19], where values of about 7 cP for η_B, and a ratio of $\eta_B/\eta_s \approx 4.2$ after melting have been measured.

It is worth remarking that, in cases like the one considered here (or Bi), estimates of the bulk viscosity using formulas linking the measured self-diffusion coefficient with the inverse of the longitudinal and shear viscosities, generally applicable to hard-sphere or Lennard-Jones (LJ) fluids (see, for instance, Ref. [20]), substantially underestimates the bulk component and, as a matter of fact, a calculation performed in such a basis led to a value for $\eta_B \approx 3.2$ cP, far below the estimates given above. The same qualifications apply to the case of liquid Bi, where experimental data regarding this transport property are available. Although the first-principles calculation of both viscosity coefficients still constitutes a formidable task, it becomes possible to estimate the ratio of the bulk to shear viscosities from the derivatives of the interparticle potential and the pair correlation function from [21],

$$\frac{\eta_B}{\eta_s} = \frac{30}{18}\frac{\int_0^\infty dr g(r) r^2 [u''(r) + u'(r)/r]}{\int_0^\infty dr g(r) r^2 [u''(r) + 4u'(r)/r]}, \quad (5)$$

where the primed quantities are derivatives of the interparticle potential (see Appendix). The calculated values of such a ratio are deemed to be far more accurate than the individual values for the two coefficients since the uncertainties in modeling the friction constant (entering as a prefactor in the two terms) are removed. A calculation from the effective potentials and partial pair correlations given in Ref. [9] yields values for such ratios of 4.71 for T=326 K and 1.16 for T=956 K, which adds further support to the values estimated from the longitudinal viscosity as commented above, since an estimate of the hydrodynamic limit of the longitudinal viscosity of 11.4 cP is obtained.

B. Inelastic scattering

As mentioned above, one of the aims of the present experiment was to test the existence of finite-frequency excitations, which, according to the calculations described in the Appendix based upon structural data and the derived effective potentials, were predicted to exist in the cold liquid. The characteristic frequencies given in terms of the $\omega_0(Q)$ and $\omega_l(Q)$ square roots of the reduced second and fourth frequency moments of the scattering law are shown in Fig. 2(a). As can be seen from the figure,

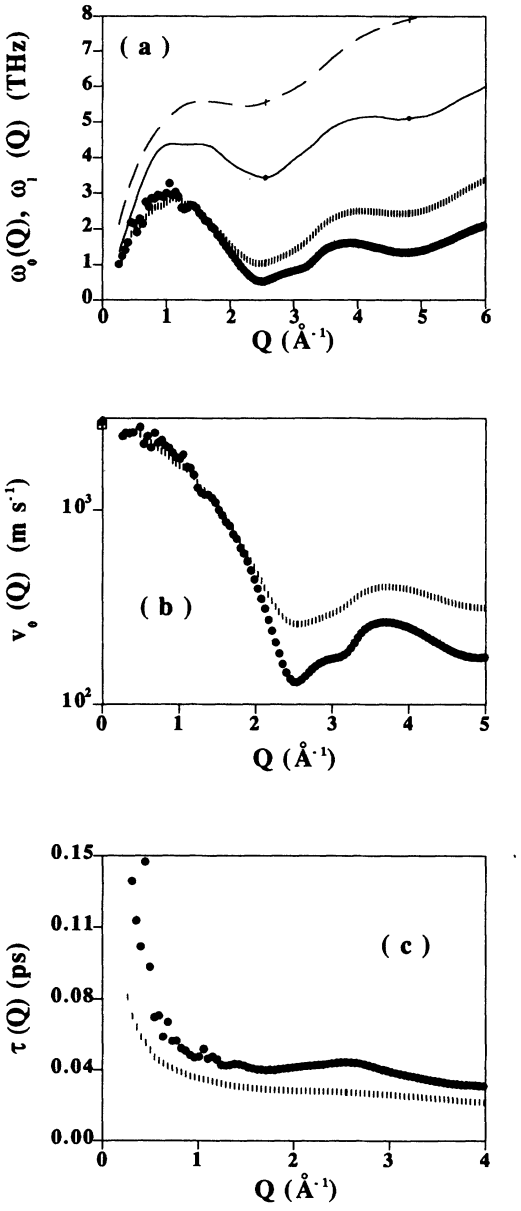

FIG. 2. (a) Calculated wave-vector dependence of the square root of the second $\omega_0^2(Q)$ and fourth $\omega_l^2(Q)$ reduced frequency moments for the two temperatures for which accurate diffraction data and effective potentials were available. Black dots and solid line represent these quantities for T = 326 K, and bars and dashed line correspond to T = 956 K. (b) The logarithm of the phase velocities as derived from the calculated second frequency moment. Filled symbols correspond to low temperature and vertical bars to the higher. The symbols in the ordinate give the hydrodynamic values for the ultrasonic (adiabatic) velocity. (c) The calculated Maxwellian relaxation times for the two temperatures considered. Same symbols as above are used.

the close proximity, at wave vectors below $Q \approx 1.7$ Å^{-1}, of ω_0 and ω_l in the cold liquid leads to the fulfillment of the condition $3\omega_0^2(Q) - \omega_l^2(Q) \geq 0$ (see Appendix), according to which finite-frequency peaks should appear in $S(Q,\omega)$ for such a range of wave vectors centered at frequencies not too far from $\omega_0(Q)$. On the other hand, as shown in Fig. 2(b), the calculated phase velocity of the excitations approaches the correct ultrasound value in the hydrodynamic limit [16], which lends some support to the calculation results. However, what comes out remarkably short are the derived Maxwellian relaxation times shown in Fig. 2(c) [22], where, for comparable wave vectors the interparticle separations become of the order of 10^{-14} s, a time scale too short in regard to thermal motion effects, but comparable to Drude relaxation times, as well as to the characteristic times for the formation of covalent aggregates, as reported from recent density-functional calculations [4].

A representative sample of the measured spectra for the two sets of incident wave vectors (uncorrected for resolution effects), is shown in Fig. 3, and are compared to the theoretical prediction upon folding the calculated spectra with the measured resolution function corresponding to the higher incident wave vector. Contrary to the case of the calculated functions, no clear sign of any well defined excitation can be found within the explored range of energy transfers, although the inelastic intensity extends up to frequencies far higher than those characteristic of self-motion (quasielastic scattering), a fact which can be easily tested by calculation of the single-particle response using the reported values of the macroscopic self-diffusion coefficients [23]. Also, the relative importance of the quasielastic term is, as expected, strongly underestimated in the theoretical spectrum.

To analyze the experimental spectra, consideration was made of both coherent-quasielastic and inelastic contributions so that the model function becomes

$$S_{\text{model}}(Q,\omega) = [S_{\text{qel}}(Q,\omega) + S_{\text{inel}}(Q,\omega)] \otimes R(Q,\omega), \tag{6}$$

$$S_{\text{qel}}(Q,\omega) = \text{Re}\left[\frac{S(Q)\tilde{F}_s(Q,z)}{1+\rho_i c(Q)(iz\tilde{F}_s(Q,z))}\right]_{z=i\omega}, \tag{7}$$

$$S_{\text{inel}}(Q,\omega) = Z(Q)\frac{1}{\pi[1-\exp(-\hbar\omega\beta)]}\frac{4\omega\omega_q\Gamma_q}{(\omega^2-\Omega_q^2)^2+4\omega^2\Gamma_q^2}, \tag{8}$$

where the symbol $\otimes$ stands for convolution with the instrumental resolution function, the coherent quasielastic response is evaluated by means of the approach due to Kerr [13] in terms of the $\tilde{F}_s(Q,z)$ Laplace transform of the $F_s(Q,t)$ single-particle response (see Appendix), the static structure factor and the direct correlation function $c(Q) = (S(Q)-1)/S(Q)$. A damped harmonic oscillator given in terms of the $Z(Q)$ excitation strength and the Ω_q renormalized excitation frequency and Γ_q damping factor is used to represent the inelastic background. In order to reduce the number of fitting parameters, two different approaches were followed to model $S_s(Q,\omega)$, from either macroscopic transport properties or from quantities calculated from the effective potential as described in the Appendix. A first-order mode-coupling expression was used in the first case following de Schepper [24], which needed as input data regarding the macroscopic self-diffusion coefficient and kinematical viscosity, and the three-pole expression for the incoherent function was constructed from its first two even frequency moments, following the usual formulas [22]. Although some differences are expected to show as a consequence of the use of such models (the first one is not valid for large wave vectors), the calculated linewidths are well below the achieved experimental resolution, so that no significant information could be drawn from the present experiments. The calculated functions merit, however, some further consideration regarding the thermal and transport processes as described below.

Even if no finite-frequency features are visible in the spectra, the renormalized frequencies $\Omega_q = \sqrt{\omega_q^2 + \Gamma_q^2}$ [25] can be interpreted as true excitation frequencies of an oscillator undergoing overdamped motion. As a matter of fact, as Fig. 4 shows, the derived values of such magnitudes can be favorably compared with the calculated ones, at least within the kinematic range useful for such a comparison (i.e., 1.2–3.5 Å^{-1}). The fitted values for these frequencies seem to lie systematically above those of the second moment curve, which may be interpreted as an indication that inelastic intensities arising from higher-lying optic modes contribute substantially to the spectra, thus causing a pullout toward higher values. Such an hypothesis seems to be consistent with estimates of the frequency distribution, as will be shown below.

The origin of such large damping terms can explained from consideration of the viscous contribution only (the heat conduction term can, in principle, be neglected due to the small value of $\gamma - 1$, and can only be relevant if the latter quantity exhibits a strong dependence on the wave vector). A simple calculation in hydrodynamic terms of the damping ratio following

$$\Gamma_q^{\text{calc}} = \frac{4/3\eta_s + \eta_B}{2\rho_i}Q^2 \tag{9}$$

reveals that if the estimates of the longitudinal viscosity shown in Fig. 1 are taken, values for the damping constant of about 1.5 THz from the calculated curve and of 3.2 THz from the experimental points are found for the range of wave vectors of interest ($Q \approx 1$ Å^{-1}). The high value of the damping constant corresponding to the

experimental data becomes some 0.4 THz higher than the predicted value of the ω_0 excitation frequency, thus preempting the appearence of any resolved peaks in the corresponding dynamical structure factor.

Further support for the existence of collective excitations is demonstrated by the inelastic structure factors taken at constant energy transfer shown in Fig. 5. The data can be favorably compared with those of Löffler [10] measured a long time ago, since the statistical accuracy achieved in the present measurement is far better. Some relevant information regarding the microscopic origin of the excitations being sampled can be derived from the relative phases of the oscillations, if a dynamical model is available. Unfortunately, only rather simplified constructs have been derived from either kinetic or phenomenological approaches, which cannot take due account of the complicated microscopic dynamics of this liquid. Under such circumstances, we compare the wave-vector dependence of the inelastic intensity with a model developed to account for plane wave excitations in an isotropic solid medium [26] given by

$$I(Q,\omega) \propto \frac{\hbar Q^2}{4m_i}\frac{Z(\omega)}{\omega}[n(\omega)+1]\int_{-1}^{1} d\mu\, S(Q+q_\omega\mu), \tag{10}$$

where the frequency distribution was taken to be the calculated one, the experimental static structure factor [9] is used for the calculation, and $q_\omega = \omega/v_0(Q)$ is the excitation wave vector calculated from the computed phase velocity. Although such a model is a clear idealization since mass-diffusion effects are neglected, its use can be justified for energy-transfers well above those characteristic of low-energy (quasielastic) scattering, where the response of the liquid may be not too different from a solid. A comparison between measured and calculated quantities can be seen in Fig. 5. Even admitting the crudeness of such an approach, the comparison is surprisingly adequate up to energy transfers of 3.6 THz, disregarding the mismatch in amplitudes, which is a consequence of the peaked $Z(\omega)$ used for the calculation. Most of the observed features are reproduced in the calculated curves, including the progressive loss of coherence in going from 1.25 THz to 3.6 THz of energy transfers. The strong oscillation that appears at about 3.8 Å^{-1} from 3.6 THz onward is poorly reproduced by the model calculation, which could be expected, since such frequencies are high above the maximum of the $\omega_0(Q)$ curve shown in Fig. 2(a) and, therefore, such features should correspond to excitations of optical origin.

The relatively high frequencies found in the present

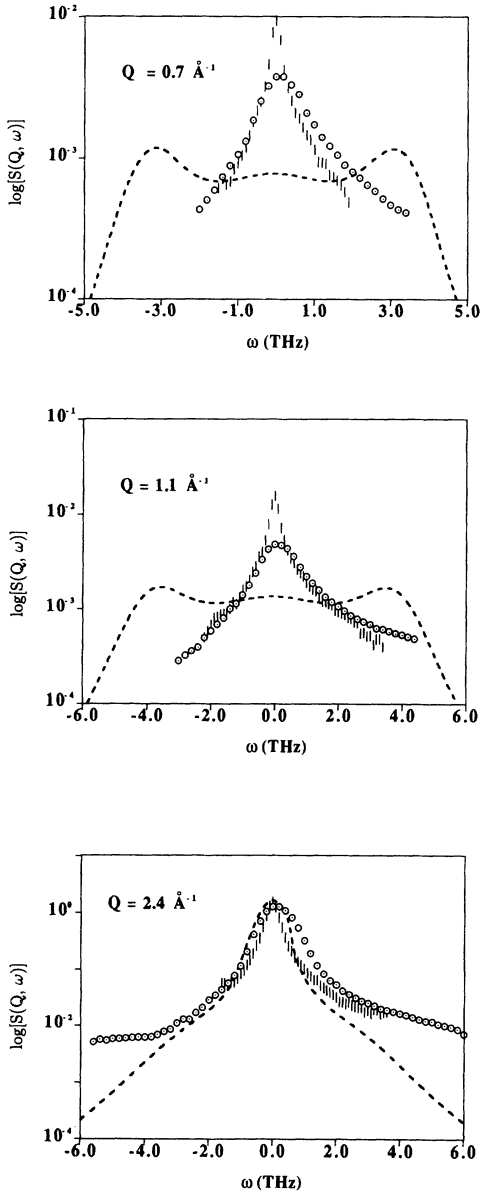

FIG. 3. Constant-Q spectra measured using the two different incident wave vectors for Q values given as insets. Vertical bars correspond to measurements with $k_f = 2.66$ Å^{-1}, and circles to those measured with $k_f = 4.03$ Å^{-1}. The dashed line represents a calculation detailed in the Appendix convoluted with the resolution function of the higher wave-vector transfer measurement.

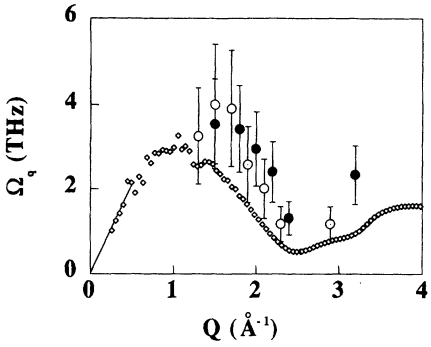

FIG. 4. A comparison between the Ω_q renormalized frequencies estimated from model fits to the inelastic intensities (symbols) with the calculated second reduced moment. Open circles are data measured using $k_f = 2.66$ Å^{-1} and filled circles stand for measurements carried out with $k_f = 4.03$ Å^{-1}. The lozenges show the calculated $\omega_0(Q)$, and the adiabatic sound velocity is depicted as the linear dispersion law given by the dashed line.

study can be easily understood if consideration is made of the vibrational spectrum investigated in the solid phase ($T = 77$ K) by Waeber [27], where 12 modes arising from the motions of the four atoms per unit cell have been observed, covering a frequency region up to ≈10 THz. As evidenced in previous works on more complex liquids [28], the spectral weight of the higher-frequency opticlike excitations becomes dominant even for relatively low wave vectors (above $\approx Q_p/4$ in both cases, where Q_p stands for the position of the first diffraction peak). Under such circumstances, most of the spectral intensity measurable using conventional instrumentation (i.e., for wave vectors of $Q \approx 1$ Å^{-1} in order to cover a significant kinematic range) will be dominated by these high-frequency components, which, due to their very nature, tend to be strongly localized.

The shape of the wave-vector dependence of the excitation curves up to ≈ 3 Å^{-1} can be well reproduced using simplified treatments such as that of Bathia and Singh [29], provided that the relative contributions of the ions and electrons to this property are taken as adjustable parameters along with k_F, which tends to require values about 10% larger than those calculated from the electronic number density. As a matter of fact, a calculation of the bulk modulus using Eq. (12) of Ref. [29] in terms of a free-electron result gives a value some 27% higher than the observed one, while the same calculation using only the ionic contribution fails to reproduce adequately the shape of the excitation curve.

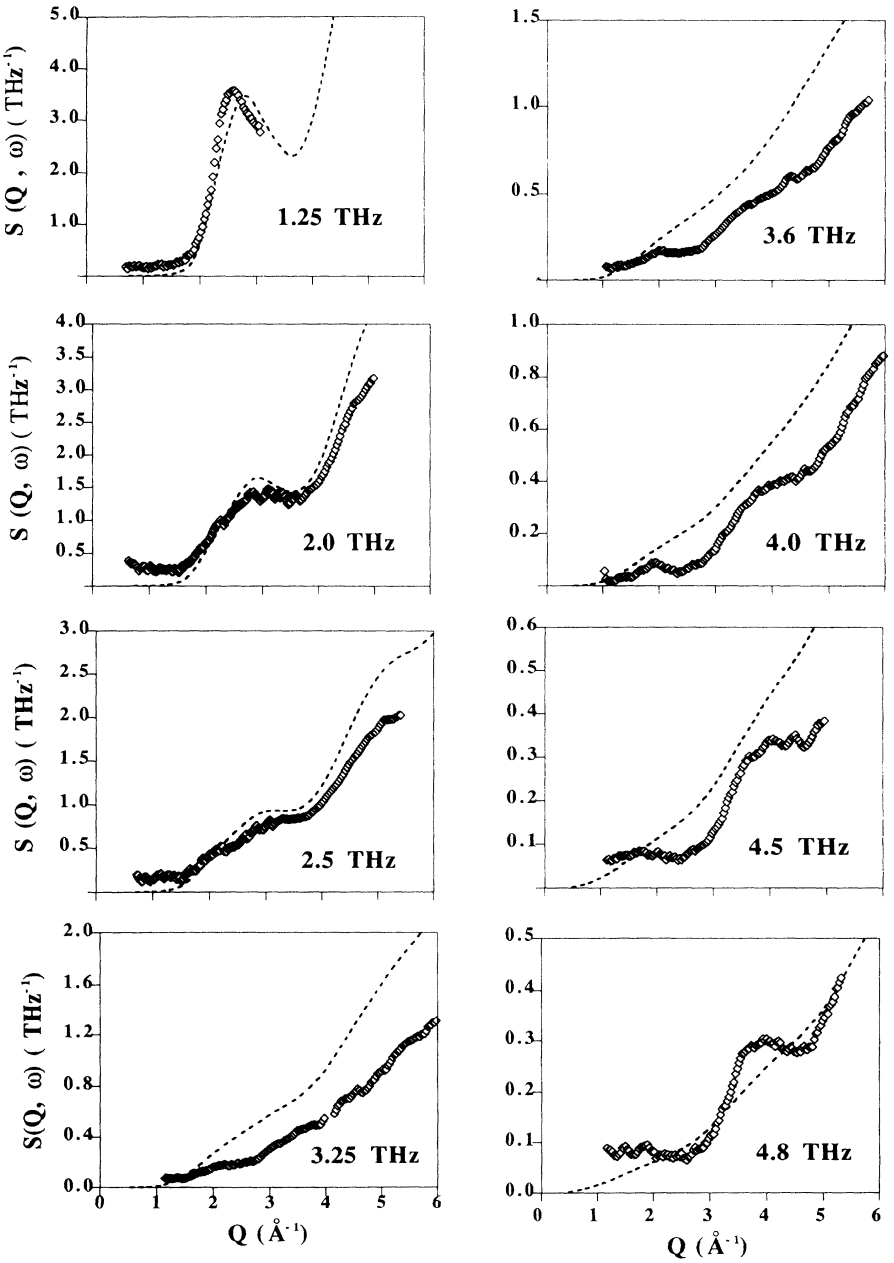

FIG. 5. Inelastic intensities at constant energy transfers (given as insets). Experimental data are shown as open lozenges and the dashed line represents the inelastic intensity as calculated using Eq. (10).

C. Electronic and thermal transport

The purpose of this section is to evaluate, using the information regarding the atomic dynamics gathered in preceding sections, the contributions to the electrical resistivity arising from diffusive and high-frequency motions. Such an exercise enables the separation of the two contributions to this transport property, which may be associated with incoherent scattering from the cores and from collective oscillations, which often exhibit rather disparate dependences with temperature. Our aim here is to explain the small value found for the temperature coefficient and, therefore, a semiquantitative treatment to evaluate this property seems adequate. The electrical resistivity was calculated from

$$\rho = \rho_{\mathrm{qel}} + \rho_{\mathrm{inel}} = \frac{m_e^2}{12\pi Z e^2 \rho_i^3 \hbar^3} \int_0^{2k_F} |V(Q)|^2 S'(Q) Q^3 dQ, \tag{11}$$

$$S'(Q) = \int_{-E_0}^{E_0} n(\omega)\beta\hbar\omega S(Q,\omega), \tag{12}$$

$$S(Q,\omega) = S_{\mathrm{qel}}(Q,\omega) + S_{\mathrm{inel}}(Q,\omega), \tag{13}$$

where m_e is the electron mass, e its charge, and a cutoff value of E_0 15 THz was used in the integrations, which allows a consideration of scattering of inelastic origin (the original formula is recovered in the high-temperature limit), as well as considerations of the contributions to the resistivity arising from stochastic (qel) and vibrational (inel) motions. The coherent response has thus been subdivided into quasielastic and inelastic terms which are evaluated using the formulas given above. The high-temperature experiment of Bellissent-Funel *et al.* [9] was also analyzed, using, for the purpose, estimates of the diffusion coefficient from [23], and the inelastic contribution was evaluated from the difference between $S(Q)$ and the integral over the quasielastic response, which can be safely done since at this temperature (956 K) the detailed-balance terms are very close to one. Several model potentials to represent the $V(Q)$ electron-ion interaction were tested [30] and the resulting calculated values for the electrical resistivity are compared with relevant experimental data in Table I. As expected, the calculated values are strongly dependent upon the pseudopotential used, an unavoidable fact unless real-space calculations such as those of Bose, Jepsen, and Andersen [31] are carried out, although the result can be compared with experiment on a semiquantitative basis. The most remarkable finding regarding this transport property concerns the rather different temperature dependence of the quasielastic and inelastic contributions, since the former decreases steadily with temperature, whereas the opposite behavior is found for the latter quantity, which shows a strong increase with temperature. Such a result, which goes counter to what has been predicted to occur in amorphous solids (see Jäckle and Fröbose in Ref. [26]), can be easily understood from consideration of the large diffusion coefficients at high temperatures (of the order of about 2 $\text{Å}^2\,\text{ps}^{-1}$ at 950 K), which result in a distribution of the spectral power covering a broader range of frequencies than those of the vibrational excitations, which makes the latter a far more efficient mechanism for electron scattering. At any rate, the calculated temperature coefficient is in acceptable agreement with published estimates, which quote values of 0.14 at temperatures about the melting point. From inspection of the numerical values given in Table I, it becomes clear that for temperatures near the melting point, the dominant electron-ion scattering mechanism has to be associated with motions involving long-range translational diffusion. Such a result could lead one to think about the significance of the inelastic term and try to relate such values to those of the hot solid. The large scatter of the numerical values introduced by the different potentials prevents any accurate estimation of such a contribution. On qualitative grounds, the values quoted in Table I can be compared with estimates of the ratio of change in resistivity on melting $\rho_{\mathrm{liq}}/\rho_{\mathrm{sol}}$ quoted in Table 5.1 of Ref. [32], giving, as a consequence of the strong anisotropy in the solid, values within the range 0.45–3.1 (i.e., 8.4–57 $\mu\Omega\,\mathrm{cm}$). The largest value for ρ_{inel} at the low temperature is not too far below the lower limit of the resistivities of the solid, although values calculated using the empty core (EMC) and Fröbose-Jäckle (FJ) pseudopotentials seem definitely too low. The smallness of the ρ_{inel} value compared with the solid could then be rationalized if additional scattering mechanisms present in the crystal (i.e., electron scattering from low-lying transverse acoustic modes) disappear upon melting (that is, such modes become unstable).

TABLE I. Calculated values for the quasielastic ρ_{qel} and inelastic ρ_{inel} contributions to the electrical resistivity ρ for the two temperatures for which the effective potential is available. Units are $10^{-6}\ \Omega\,\mathrm{cm}$. The row EMC are calculations using the empty-core model, FJ stands for the simple form of the potential employed by Fröbose and Jäckle [26], and HA corresponds to results using the Heine-Animalu pseudopotentials with a dielectric function given by Leavens [35].

	T = 326 K				T = 956 K		
Pseudopotential	ρ	ρ_{qel}	ρ_{inel}	$\frac{T_{326}}{\rho_{326}}\left[\frac{\partial\rho}{\partial T}\right]$	ρ	ρ_{qel}	ρ_{inel}
EMC	23.3	21.9	1.4	0.19	32.1	16.4	15.7
FJ	19.8	18.6	1.2	0.12	20.8	11.6	9.2
HA	25.6	19.9	5.6	0.14	34.8	13.9	20.9

The calculated $Z(\omega)$ generalized frequency distribution is finally compared with the experimental result regarding the $P(Q,\omega)$ function in Fig. 6. Both curves cover a similar range of frequencies, the main differences being located at low frequencies, as expected from the definition of $P(Q,\omega)$, as well as at higher frequencies, where the experimental curve decays more smoothly as a consequence of the intensity arising from higher-lying vibrational states, which cannot be taken into account within the simplified model employed for the calculations. From consideration of the characteristic frequencies for soundlike excitations shown in Fig. 2(a), as well as from the time scales characteristic of mass diffusion, it becomes clear that at frequencies about the maxima of those curves, the vibrational states that contribute most to the distributions cannot be identified with either of the two processes just described.

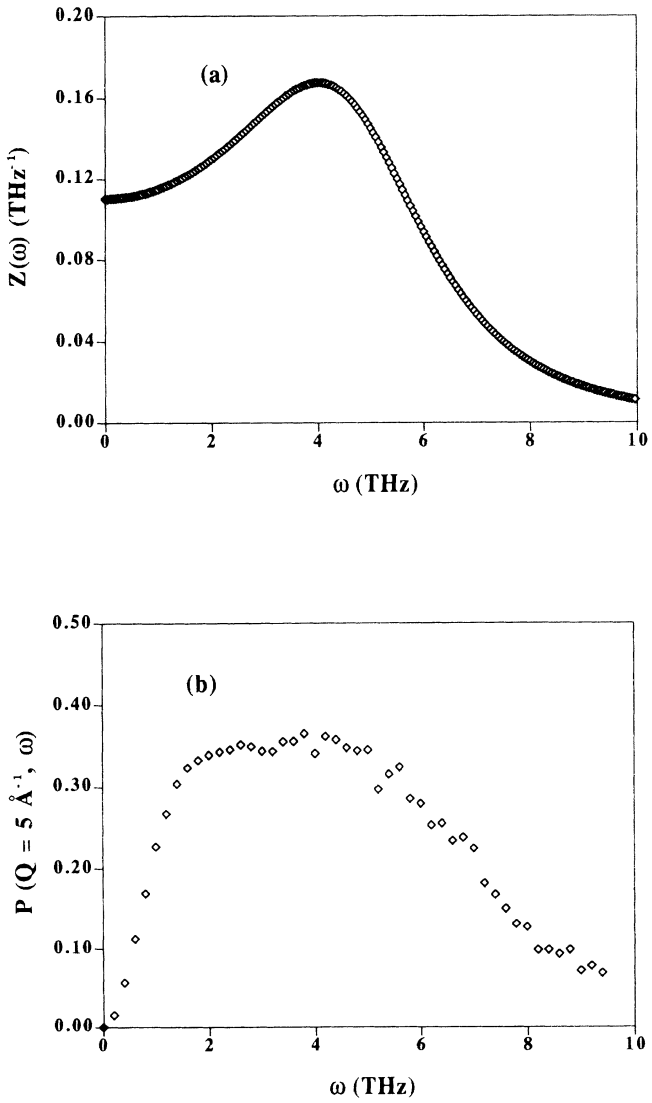

FIG. 6. (a) The generalized frequency distribution as calculated from the Fourier transform of the velocity autocorrelation function (see Appendix). (b) The function $P(Q,\omega)$ as calculated from experimental data for a momentum transfer value of 5 Å^{-1}.

The shape of the theoretical function is somewhat reminiscent of that reported for liquid sodium [33], exhibiting a clear maximum at frequencies substantially higher (about 1 THz) than those assignable to soundlike excitations. In this respect, it is appealing to consider the resemblance of the spectra of the liquid to those of the solid, an exercise which can be easily done for Na [33], and will give as a result, the close proximity of the frequency of the maxima in the liquid to that corresponding to a strong optical peak in the solid. On the other hand, it is instructive to recall the case of liquid Rb, where the maximum of its frequency distribution occurs at about 0.8 THz, without exhibiting significant contributions at far larger frequencies.

A semiquantitative estimate of the heat capacity at constant volume from the calculated frequency distribution (assuming that it represents harmonic motions), yields a value of $2.9R$ (in units of the gas constant R), to which $0.025R$ can be added from the electronic contribution calculated from the linear term of the specific heat in the solid. This value is somewhat lower than that of $3.2R$ [34], which should not be surprising considering the crudeness of the estimate [34]. A similar estimate for the entropy gave a value of $3.59R$, well below the estimate of $4.95R$ calculated from the high-temperature expansion in terms of the Debye temperature.

IV. CONCLUSIONS

From the analysis of the inelastic-neutron-scattering spectra described above, it is found that this liquid cannot sustain finite-frequency excitations analogous to those exhibited by some molten alkali metals or metals of relatively low sound velocity. Such overdamped behavior seems to be caused by the interplay of two effects, the relatively high longitudinal viscosity and the existence of a frequency spectrum covering a large range of frequency space. The latter implies that, as evidenced by the inelastic structure factors, excitations of nonsonic origin contribute significantly to the inelastic intensity for energy transfers just above the maximum of the $\omega_0(Q)$ curve. Under such circumstances it becomes clear why the predictions made by use of generalized hydrodynamics treatments, which have proven to be successful for the analysis of molten alkali metals such as Rb, are not borne out by experiment.

The decomposition of the calculated values for the electrical resistivities into diffusive and vibrational contributions, serves to disentangle the often puzzling behavior of the temperature dependence of this property. As shown, both dynamical structure factors contribute to this transport coefficient in a disparate way, showing the dominance of low-frequency motions at temperatures not too far above melting, a situation which is reversed at high temperatures.

ACKNOWLEDGMENTS

This work was supported in part by DGICYT Grant No. PB92-0114-C04. The authors wish to thank Dr. M. C. Bellisent-Funel for making available the details con-

cerning the experimental structure factors and the effective potentials. The Laboratoire Commun is Unité associée au Centre National de la Recherche Scientifique.

APPENDIX

The first two reduced even-frequency moments of $S(Q,\omega)$ are calculated within the classical approximation following [22]

$$\omega_0^2(Q) = = \frac{\langle\omega^2\rangle}{S(Q)} = \frac{Q^2}{m_i\beta S(Q)}, \tag{A1}$$

$$\omega_l^2(Q) = \frac{\langle\omega^4\rangle}{\omega_0^2} = \frac{3Q^2}{m_i\beta} + \Omega^2(0) - \Omega^2(Q),$$

$$\Omega^2(0) = \frac{4\pi\rho_i}{3m_i}\int_0^\infty r^2 dr g(r)[u''(r) + 2u'(r)/r], \tag{A2}$$

$$\Omega^2(Q) = \frac{4\pi\rho_i}{m_i}\int_0^\infty r^2 dr g(r)[u''(r) f_1(Q) - \frac{2u'(r)}{r} f_2(Q)],$$

where the primes over the $u(r)$ effective potential indicate the order of the derivative taken wrt the interatomic separation, $f_{1,2}(Q)$ are simple geometrical factors [22] and the rest of the symbols retain their usual meaning. The elastic properties given in terms of the bulk and rigidity moduli are also calculated from the structural information and the potential as

$$B + (4/3)G = \frac{3\rho_i}{\beta} + \frac{2\pi n_i^2}{5}\int_0^\infty r^2 dr g(r) \times [r^2 u''(r) + (2/3) r u'(r)], \tag{A3}$$

$$G = \frac{\rho_i}{\beta} + \frac{2\pi\rho_i^2}{15}\int_0^\infty r^2 dr g(r)\frac{\partial(r^4 u'(r))}{\partial r}. \tag{A4}$$

The isothermal compressibility and the B_T modulus are calculated from the ultrasonic velocity [16] after allowance is made for the small correction due to the ratio of specific heats. Within the viscoelastic theory [22], the existence of finite-frequency excitations is ensured if the condition $3\omega_0^2(Q) - \omega_l^2(Q) \geq 0$ is fulfilled, and a Maxwellian relaxation time is approximated by $\tau = (2[\omega_l^2(Q) - \omega_0^2(Q)]/\pi)^{-1/2}$. From the calculated frequency moments, positive values for such a difference are found in wave vectors up to ≈ 1.7 Å^{-1} in the low-temperature state, going up to a maximum of $\approx$10 THz^2 about $Q_p/2$, whereas only overdamped features can be expected to show in the high-temperature liquid. Also, the long-wavelength form of such an inequality turns out to be $3B_T/(B+4/3G) > 1$, and the calculated values for such a quantity were 2.11 and 0.78 for the low- and high-temperature liquids, respectively. Calculation of the frequency moments corresponding to self motion is straightforward, since

$$\langle\omega^2\rangle = Q^2/\beta m; \langle\omega^4\rangle = \langle\omega^2\rangle[3\langle\omega^2\rangle + \Omega^2(0)] \tag{A5}$$

and the $F_s(Q,t)$ intermediate scattering function is then evaluated from expressions given in Ref. [36]. The generalized frequency distribution is then finally calculated from the Fourier transform of the relevant velocity autocorrelation [36],

$$\psi(t) = v_{\rm th}^2 \exp(-t/2\tau)\left[\cos(\epsilon t) + \frac{\sin(\epsilon t)}{2\epsilon t}\right], \tag{A6}$$

where $v_{\rm th}$ is the thermal velocity and

$$\epsilon = \sqrt{\left[\Omega^2(0) - \left(\frac{1}{2\tau}\right)^2\right]}; \tau = [m\beta\Omega^2(0) D_T]^{-1}, \tag{A7}$$

where D_T is the macroscopic self-diffusion coefficient.

[1] W. Gläser, J. Phys. Condens. Matter **3**, F53 (1991).

[2] O. Söderstrom, U. Dahlborg, and W. Gudowski, J. Phys. F **15**, L23 (1985); O. Söderstrom, J.R.D. Copley, J.B. Suck, and B. Dorner, J. Phys. F **10**, L151 (1980).

[3] J. Hafner and G. Kahl, J. Phys. F **14**, 2259 (1984).

[4] X.G. Gong, G.L. Chiarotti, M. Parinello, and E. Tosatti, Europhys. Lett. **21**, 469 (1993); Phys. Rev. B **43**, 14 277 (1991) for a similar calculation regarding α Ga. Partial covalency effects have been repeatedly adduced as an explanation of the decrease in molar volume after melting (about 3% in Ga).

[5] Structural (x-ray) data for amorphous Ga are reported by A. Bererhi, L. Bosio, R. Cortes, A. Defrain, and C. Segaud, J. Phys. (Paris) Colloq. **41-C8**, 218 (1980). A recent molecular-dynamics simulation of the metal in the amorphous state has been reported by S.-F. Tsay, Phys. Rev. B **48**, 5945 (1993).

[6] J. Copley and J. Rowe, Phys. Rev. A **9**, 1656 (1974).

[7] T. Bodensteiner, Chr. Morkel, W. Gläser, and B. Dorner, Phys. Rev. A **45**, 5709 (1992).

[8] At temperatures near the freezing point, the ratio of specific heats amounts to $\gamma = 1.08$, and an evaluation of the effective Grüneisen constant from the ratio of the third derivative to the second of the potential taken at the potential minimum gives a value $\gamma_G \approx 0.8$. Also, values of the Lorenz number of about 2.07×10^{-8} W Ω^0 K^{-2} (i.e., well below the value of 2.45×10^{-8} W Ω^0 K^{-2} calculated for simple-liquid metals) have been reported. According to these values and to the commonly accepted diagnostic that a liquid should exhibit underdamped collective density oscillations for γ close to unity and $\gamma_G \leq 2$, well defined finite-frequency excitations could be expected to take place in this liquid.

[9] M.C. Bellisent-Funel, P. Chieux, D. Levesque, and J.J. Weis, Phys. Rev. A **39**, 6310 (1989).

[10] U. Löffler, thesis, University of Karlsruhe, 1973. Part of the data are shown in Ref. [22], p. 505.

[11] High-resolution quasielastic scattering was reported by D.I. Page, D.H. Saunderson, and C.G. Windsor, J. Phys. C **6**, 212 (1973); L. Bosio, E. Schedler, and C.G. Windsor, J. Phys. (Paris), **37**, 747 (1976). Estimates of the quasielastic widths for the temperature of interest were calculated from the temperature dependence of the linewidths given in these references.

[12] M.W. Johnson and A.E.R.E. Harwell (unpublished).
[13] W. Kerr, Phys. Rev. **174**, 316 (1968).
[14] K. E. Larsson, W. Gudowski, and M. Dzugutov, in *Static and Dynamic Properties of Liquids*, edited by M. Davidovic and A.K. Soper, Springer Series in Physics Vol. 40 (Springer, Berlin, 1989), p. 13.
[15] N.H. March, *Liquid Metals: Concepts and Theory* (Cambridge University Press, Cambridge, 1990).
[16] The density, adiabatic sound velocity, and sound attenuation data have been taken from M. Inui, S. Takeda, and T. Uechi, J. Phys. Soc. Jpn. **61**, 3203 (1992).
[17] G. Samsonov, *Handbook of The Physicochemical Properties of the Elements* (Plenum, New York, 1968).
[18] W. Gudowski, K.E. Larsson, and M. Dzugutov, in *Static and Dynamic Properties of Liquids* (Ref. [14]), p. 37.
[19] J. Jarzynski, Proc. Phys. Soc. (London) **81**, 745 (1963).
[20] R. Zwanzig, J. Chem. Phys. **79**, 4507 (1983).
[21] The original expressions for both coefficients contain prefactors $\rho_i^2/18\gamma$, and $\rho_i^2/18\gamma$, respectively, where γ is the friction coefficient, and are due to J. Kirkwood and S.A. Rice, J. Chem. Phys. **31**, 901 (1959).
[22] J.R.D. Copley and S.W. Lovesey, Rep. Prog. Phys. **38**, 461 (1975).
[23] The values for the self-diffusion coefficient as well as its temperature dependence were taken from the parametrization given by J. Bosse, D. Quitmann, and C. Wetzel, J. Phys. (Paris) Colloq. **41-C8**, 378 (1980).
[24] I. de Schepper and E.G.D. Cohen, Phys. Rev. A **22**, 287 (1980).
[25] B. Dorner, Physica B **180 & 181**, 265 (1992).
[26] Such an expression is basically equivalent to that derived by J. Jäckle and K. Fröbose, J. Phys. F **9**, 967 (1979), and also to the one used by U. Buchenau, Z. Phys. B **58**, 181 (1985), for the analysis of excitations in amorphous solids.
[27] W.B. Waeber, J. Phys. C **2**, 903 (1969).
[28] See, for instance, J. Alonso, F.J. Bermejo, M. Garcia-Hernandez, J.L. Martinez, W.S. Howells, and A. Criado, Phys. Lett. **A172**, 177 (1992) and references therein; or A. Criado, F.J. Bermejo, M. Garcia-Hernandez, and J.L. Martinez, Phys. Rev. E **47**, 3516 (1993).
[29] A.B. Bathia and R.N. Singh, Phys. Rev. **31**, 475 (1985). Notice that a contribution from single-particle motions (i.e., $\propto 3Q^2/m_i\beta$), has to be inserted in their formulas in order to recover the correct frequency moments.
[30] An empty-core model using the radial parameters given in Ref. [3] was used along with the simplified potential employed by K. Fröbose and J. Jäckle, J. Phys. F **7**, 2331 (1977). A somewhat more refined calculation used the Heine-Animalu potential: A.O.E. Animalu and V. Heine, Philos. Mag. **12**, 1249 (1965), with a dielectric function modeled following Leavens [35], using values for the mean free path of 10 Å. No corrections for the blurring of the Fermi surface were deemed neccessary.
[31] S.K. Bose, O. Jepsen, and O.K. Andersen, Phys. Rev. B **48**, 4265 (1993).
[32] T.E. Faber, *Theory of Liquid Metals* (Cambridge University Press, Cambridge, England, 1972), p. 313.
[33] Compare, for instance, the spectrum of liquid sodium shown on p. 253 of P.A. Egelstaff, *An Introduction to Liquid State Physics* (Oxford Science Publications, Oxford, 1992) with that of the solid given by A.E. Dixon, A.D.B. Woods, and B.N. Brockhouse, Proc. Phys. Soc. (London) **81**, 973 (1963).
[34] Value taken from Table 8.1 of Ref. [15]. A reliable calculation of this property requires the knowledge of three- and four-body correlation functions, which seems at present impracticable.
[35] C.R. Leavens, A.H. MacDonald, R. Taylor, A. Ferraz, and N.H. March, Phys. Chem. Liq. **11**, 115 (1981).
[36] S.W. Lovesey, *Theory of Neutron Scattering from Condensed Matter* (Oxford Science Publications, Oxford, 1986), p. 186.